A Comparison of Independent Star Formation Diagnostics for a UV-Selected Sample of Nearby Galaxies

Mark Sullivan[1,2], Bahram Mobasher[3,4], Ben Chan[5], Lawrence Cram[5], Richard Ellis[2],
Marie Treyer[6], Andrew Hopkins[7]

ABSTRACT

We present results from a decimetric radio survey undertaken with the Very Large Array (VLA) as part of a longer term goal to inter-compare star formation and dust extinction diagnostics, on a galaxy by galaxy basis, for a representative sample of nearby galaxies. For our survey field, Selected Area 57, star formation rates derived from $1.4\,\mathrm{GHz}$ luminosities are compared with earlier nebular emission line and ultraviolet (UV) continuum diagnostics. We find broad correlations, over several decades in luminosity, between Hα, the UV continuum and $1.4\,\mathrm{GHz}$ diagnostics. However, the scatter in these relations is found to be larger than observational errors, with offsets between the observed relations and those expected assuming constant star-formation histories and luminosity-independent extinction models. We investigate the physical origin of the observed relations, and conclude the discrepancies between different star-formation diagnostics can only be partly explained by simple models of dust extinction in galaxies. These models cannot by themselves explain all the observed differences, introducing the need for temporally varying star-formation histories and/or more complex models of extinction, to explain the entire dataset.

Subject headings: surveys – galaxies: evolution – galaxies: starburst – cosmology: observations – ultraviolet: galaxies – radio continuum: galaxies

[1]Institute of Astronomy, Madingley Road, Cambridge CB3 OHA, UK

[2]California Institute of Technology, E. California Blvd, Pasadena CA 91125, USA

[3]Space Telescope Science Institute, 3700 San Martin Drive, Baltimore, MD 21218, USA

[4]Affiliated with the Astrophysics Division of the European Space Agency

[5]School of Physics, University of Sydney, Sydney NSW 2006, Australia

[6]Laboratoire d'Astronomie Spatiale, Traverse du Siphon, 19976 Marseille, France

[7]Department of Physics and Astronomy, University of Pittsburgh, 3941 O'Hara Street, Pittsburgh, PA 15260, USA

1. Introduction

Considerable observational progress has been made in tracking the star formation rate (SFR) per comoving volume element as a function of redshift (see Madau et al. 1996). The form of this "cosmic star formation history" is important not only in indicating likely eras of dominant activity but also in securing a self-consistent picture of chemical enrichment for detailed comparison with intergalactic absorption line diagnostics (Pei, Fall, & Hauser 1999), as well as with the predictions of popular semi-analytical models of galaxy formation (e.g. Baugh et al. 1998; Cole et al. 2000). Various observational diagnostics have been employed to determine the SFR of a galaxy in a particular redshift survey. These include (i) Hydrogen series (i.e. Balmer or Lyman) or other nebular emission lines, generated in regions ionised by the most massive ($\gtrsim 10 \, M_\odot$) early-type stars (Gallego et al. 1995; Tresse & Maddox 1998; Glazebrook et al. 1999; Moorwood et al. 2000), (ii) the ultraviolet (UV) continuum, dominated by young (but less massive, $\gtrsim 5 \, M_\odot$) stars (Lilly et al. 1996; Madau et al. 1996; Treyer et al. 1998; Cowie et al. 1999; Steidel et al. 1999; Sullivan et al. 2000), (iii) far infrared (FIR) luminosities arising from thermal emission from dust absorbed UV radiation from the more massive stars (Rowan-Robinson et al. 1997; Blain et al. 1999), and (iv) 1.4 GHz radio emission, thought to originate mainly via synchrotron radiation generated by relativistic electrons accelerated by type II supernovae (SNe) from stars of mass $\gtrsim 7 - 8 \, M_\odot$ (Condon 1992; Cram et al. 1998)

Each diagnostic has its own merits, disadvantages and uncertainties (for a review see Kennicutt 1998) and none can yet be applied uniformly to samples over the full observed redshift range. Accordingly, it is inevitable that the cosmic star formation history (SFH) has been pieced together using different diagnostics from independent samples of galaxies. Therefore, it is crucial to know how well the various diagnostics agree *on a galaxy by galaxy basis.* A major source of uncertainty is the likelihood that some diagnostics are affected by the presence of obscuring dust. Radio continuum diagnostics have the distinct advantage of being immune from dust extinction. Non-uniformities in the SFH (or a time varying SFR) are also important, and might, if present, introduce additional biases between the different SFR diagnostics.

Only limited work has been done inter-comparing different star-formation (SF) diagnostics for galaxies, with studies at low and intermediate redshifts showing significant discrepancies. Cram et al. (1998) compared the SFRs from Hα, FIR and U-band measurements with those from decimetric radio luminosity ($L_{1.4}$) for a sample of over 700 local galaxies. Though the various SFR estimates were in broad agreement, numerous systematic differences were found, including a significant scatter in all the relationships compared to the $L_{1.4}$/FIR relation. They conclude that the scatter may partly be due to sample selection

(i.e. inhomogeneities in the sample selection or possible AGN contamination) or have a real physical basis (e.g. differential extinction among individual galaxies or time-dependent initial mass functions). Studies comparing UV continuum and Hα emission fluxes likewise reveal systematic discrepancies and a large scatter (Glazebrook et al. 1999; Sullivan et al. 2000; Bell & Kennicutt 2001). Although extinction is a likely source of the scatter, Sullivan et al. (2000, hereafter S2000) argued that the observed trend on the UV-Hα plane is consistent with non-uniform SFHs for some fraction of the population. If starburst activities are a common occurrence for high redshift galaxies as some models suggest (Somerville, Primack, & Faber 2001), further corrections may be needed to derive representative SFRs from optical and UV diagnostics based on luminous sources only.

This paper is motivated by the need for more comprehensive and rigorous investigation into the inter-relationships between the various SF diagnostics, including those based on the promising 1.4 GHz luminosity. Though the radio emission is generally thought to be generated as a by-product of the supernovae of massive stars (and therefore a measure of SFR), the steps relating the supernovae explosion to the arrival of radio emission at the Earth – for example the electron acceleration in the supernova remnant and the subsequent cosmic ray propagation, the role of magnetic fields, any possible energy loss mechanisms, or a significant cosmic-ray escape fraction – are not yet well understood. We are therefore particularly interested in the quantitative empirical precision with which radio luminosities can be used to trace SF. The major hurdle is the need for a large, well-controlled sample with considerable overlap in the various diagnostics. For this study, we choose the UV-selected sample discussed by Treyer et al. (1998) and S2000, drawn from the FOCA balloon-borne imaging data of Selected Area 57 (SA57), taken by Milliard et al. (1992). The SA57 survey contains 222 spectroscopically-confirmed star-forming galaxies, forming a statistically-complete sample selected at 2000 Å.

A plan of the paper follows. In §2 we review the SA57 dataset and briefly describe the 1.4 GHz observations (a more detailed description will be given by Chan et al., in preparation). In §3 we discuss the adopted flux-SFR calibrations, the selection effects present in our sample, and inter-compare the SFRs derived from the different diagnostics. In §4 we discuss the implications and present our conclusions. Throughout we assume $\Omega_{\mathrm{M}} = 1$, $H_0 = 100 \, \mathrm{km \, s^{-1} \, Mpc^{-1}}$, solar metallicity, and, unless otherwise stated, our adopted initial mass function is Salpeter (1955)-like ($\Psi(M) \sim M^{-2.35}$) with mass limits $\mathrm{M_{lower}} = 0.1$ and $\mathrm{M_{upper}} = 100 \, \mathrm{M_\odot}$.

2. The Datasets

The UV-selected sample is drawn from the Milliard et al. (1992) FOCA 1500 1.55° diameter image of Selected Area 57 centered at RA = $13^h03^m53^s$, Dec. = +29°20′30″ (B1950). The photometric details are presented in Treyer et al. (1998) and S2000. Briefly, the errors in the UV photometry range from 0.2 mag at the bright end to 0.5 mag at the fainter end. Optical fiber spectroscopy has been secured for an unbiased (i.e. randomly selected) subset of 369 UV sources limited at $m_{UV} = 18.5$ (equivalent to $B \simeq 20 - 21.5$ for a late-type galaxy) using the WIYN observatory[1] ($\lambda\lambda = 3500 - 6600$ Å) and the William Herschel Telescope (WHT, $\lambda\lambda = 3500 - 9000$ Å). This spectroscopy provides redshifts for 222 UV-selected galaxies, of which 178 were found to have strong emission line spectra. However, only the WHT spectra have sufficient wavelength coverage to detect Hα, and only for a subsample of 88 WHT-observed galaxies is the flux calibration sufficient for a reliable conversion of Hα to SFR (note this does *not* include all the galaxies with detected Hα emission). The errors in the Hα fluxes are estimated from the S/N of the spectrum in question. A fiber size of 2.7" diameter was used for the flux-calibrated optical spectroscopy; no aperture corrections are applied, hence the Hα flux is underestimated in very nearby objects with a larger apparent size (see S2000).

The 1.4 GHz radio observations were carried out at the NRAO VLA telescope, and cover the central square degree of the SA57 field. A 4σ detection limit of 170 μJy was achieved at the centre of the field dropping to 340 μJy in the outer regions. A detailed discussion of the VLA radio data and its reduction will be presented in Chan et al. (in prep.). Briefly, the task is to measure radio flux densities, or to estimate upper flux limits, at the positions of all the FOCA-UV galaxies. This problem is not the same as deriving a catalogue from the image, since the search positions, at which the FOCA galaxies are located, are pre-determined. The position-dependent noise in the image, arising from the primary beam response and the mosaicing method, complicates this problem. We begin by constructing an image of the position-dependent noise, using the measured noise near the centers of the pointings in conjunction with the primary beam attenuation and the overlapping of the mosaic. We then search near each UV position. For radio sources with flux densities greater than 4σ, we use the AIPS task VSAD to determine the source properties from a one-component Gaussian fit in which the amplitude, size and position of the source is allowed to vary. Three of these fits reveal very extended sources, whose properties were recalculated from the individual pixel values. For sources fainter than 4σ, a Gaussian fit was made with the position fixed

---

[1]The WIYN Observatory is a joint facility of the University of Wisconsin-Madison, Indiana University, Yale University, and the National Optical Astronomy Observatories.

at the UV source position using the MIRIAD task IMFIT (as VSAD does not allow position-fixed fitting). If the amplitude of this fit exceeds the local 1σ noise level, it is reported as a detection, while fainter fits are reported as upper limits using the 1σ level. For all reported fits, the 1σ error is reported based on the noise image.

A total of 26 out of 191 FOCA galaxies (with a secure redshift) within the central $1.4\,$GHz survey area of SA57 are detected using VSAD at a significance level of $\geq 4\,\sigma$. Of these, 22 have single optical counterparts on the Palomar Sky Survey (POSS) plates (see S2000 for a discussion of FOCA/POSS identification procedures). A further three FOCA sources were identified with extended radio emission that provided poor fits to a Gaussian profile; the fluxes for these were consequently calculated by adding together all the pixels inside the extended emission area as described above. The position fixed fitting identifies a further 25 galaxies, 18 with unambiguous optical counterparts. Since in the present paper we only wish to study field galaxies (avoiding contamination by known cluster members which are likely to reside in different environments), we also exclude 3 galaxies in the redshift range of the nearby Coma cluster ($0.020 < z < 0.027$). A summary of the sample numbers is given in Table 1. Of the final sample, 25 WHT-observed galaxy spectra have detected Hα of which 17 have an adequate flux calibration to derive SFRs.

All observed radio luminosities have been k-corrected to luminosities appropriate to a rest-frame frequency of $1.4\,$GHz according to $L_{1.4}^0 = L_{1.4}^{obs} \times (1 + z)^{-0.8}$, where the spectral index of -0.8 is typical for the non-thermal synchrotron component of decimetric radiation.

3. Inter-comparison of star formation diagnostics

3.1. Diagnostic Relations

To compare the SF diagnostics based on the radio ($L_{1.4}$), UV (L_{uv}), and Hα ($L_{H\alpha}$) luminosities, a self-consistent calibration is required. This is accomplished using the PEGASE-II spectral synthesis code (Fioc & Rocca-Volmerange 1999) which generates galaxy spectra as a function of time for arbitrary SFHs, from which the Hα and UV luminosities can be calculated (S2000). In order to estimate $1.4\,$GHz luminosities for a given SF scenario, we add a simple prescription using the type II supernovae rate given by PEGASE-II, using calibrations from Condon (1992). We calculate the conversion factors for four of the different metallicities available in PEGASE-II; we report solar metallicity conversions below, and the remainder in Table 2. Assuming a constant SFH, the three SF diagnostics in this study are calibrated as explained below:

Hα emission: The relevant photons originate via re-processed ionizing radiation at wave-

lengths $\lambda < 912\,\text{Å}$ produced by the most massive ($> 10\,\text{M}_\odot$), short-lived ($\simeq 20\,\text{Myr}$), OB stars. Accordingly, Hα emission is a virtually instantaneous SF measure – for a burst of star-formation with a constant SFR, the Hα emission can be considered constant after $\simeq 10\,\text{Myr}$. However, as it depends so strongly on the most massive stars, it is very sensitive to the form of the initial mass function (IMF) (see Kennicutt 1998, for example). There is much debate in the literature as to the universality, or otherwise, of the IMF (see Scalo 1998; Gilmore 2001; Eisenhauer 2001, for recent reviews); here we assume the form to be universal, but discuss variations in the upper mass cut-off in Section 4.3. Most calibrations assume case-B recombination (a comprehensive treatment of its use can be found in Charlot & Longhetti 2001). Using PEGASE-II we derive:

$$SFR = \frac{L_{H\alpha}(\text{erg s}^{-1})}{1.22 \times 10^{41}} \; \text{M}_\odot \; \text{yr}^{-1}. \tag{1}$$

As a comparison, Kennicutt (1998) derive a conversion value of 1.26×10^{41}, very close to the value used here.

UV 2000 Å continuum: As stars that contribute to radiation at $2000\,\text{Å}$ span a range of ages (and hence initial masses), including some post-main sequence contribution, any UV-SFR calibration is dependent on the past history of SF. This introduces a significant uncertainty when interpreting the observations of the star-forming galaxies in this sample. As a guide, we calculate conversion values based on constant burst of SF of durations 10, 100 and 1000 Myr using PEGASE-II. This gives:

$$SFR = \frac{L_{UV}(\text{erg s}^{-1}\,\text{Å}^{-1})}{x \times 10^{39}} \; \text{M}_\odot \; \text{yr}^{-1}. \tag{2}$$

where x is equal to 3.75, 5.76 and 6.56 for 10, 100 and 1000 Myr respectively. Kennicutt (1998) derive a conversion value of 5.36×10^{39}, again in good agreement.

1.4 GHz continuum: The integrated radio flux at $1.4\,\text{GHz}$ is thought to originate via non-thermal synchrotron emission from electrons accelerated by supernovae (spectral index $\simeq -0.8$) and thermal Bremsstrahlung from electrons in ionised H II regions (spectral index $\simeq -0.1$). Non-thermal emission dominates (around 90%) at the frequency of interest. We introduce a prescription into PEGASE-II to predict the non-thermal $1.4\,\text{GHz}$ luminosity, $L_{1.4}$, based on the radio supernova rate (type II SNe) in the PEGASE-II code. For a constant SFR burst, the SNe II rate is effectively constant after $\simeq 80\,\text{Myr}$. Using the relationship between non-thermal radio luminosity and the radio supernova rate, presented in Condon & Yin (1990) (see also Condon 1992), the SFR as a function of $1.4\,\text{GHz}$ luminosity for our assumed IMF is:

$$SFR = \frac{L_{1.4}(\mathrm{erg\,s^{-1}\,Hz^{-1}})}{x \times 10^{27}} \; \mathrm{M}_\odot \; \mathrm{yr}^{-1}. \tag{3}$$

where x is equal to 2.39 and 8.85 for 10 and 100 Myr respectively. This agrees well with a conversion factor of 7.36×10^{27} given by Haarsma et al. (2000), which maps non-thermal luminosity to SFR at 1.4 GHz. The small difference arises as PEGASE-II calculates a smaller (metallicity dependent) lower mass cut-off for type II SNe than the $8\,\mathrm{M}_\odot$ used in Condon (1992), as convective overshooting increases the mass of the degenerate core, and the Chandrasekhar mass is reached more easily (M. Fioc 2000, private communication), hence the conversion factor above is slightly metallicity dependent (see Table 2). We neglect the small amount of thermal emission at 1.4 GHz.

There is some evidence to suggest that the calibration of $L_{1.4} - SFR$ may not be perfectly linear, particularly in low luminosity (or low SFR) objects where there is the possibility that a fraction of the SN remnant-accelerated cosmic rays may escape from the galaxy (Condon, Anderson, & Helou 1991). In such scenarios, the true SFR for a galaxy may be underestimated when using the linear relationship presented above.

Our 'standard' scenario then uses the calibrations listed above, and the following implicit assumptions: i) constant SFHs over recent timescales for the galaxies under study, ii) a Salpeter IMF, iii) solar metallicity and the stellar libraries/evolutionary tracks used in PEGASE-II (Fioc & Rocca-Volmerange 1999), and iv) a simple, tight and linear relationship between $L_{1.4}$ and SFR. We will discuss the validity of some of these assumptions in later sections.

3.2. The effects of selection bias

Before analysing the present dataset in more detail, it is important to explore possible selection effects that might operate in any comparison where only a subset of one diagnostic set is used. In particular, we need to determine that any correlations seen in our data are not merely products of the potentially complex selection effects in this study. In this section we attempt to identify which types of galaxies are excluded from our combined survey due to the different flux limits, and how this might affect any correlations that we see in our data.

Our sample has two independent flux limits. The first arises from the original selection at 2000 Å, which was limited at $m_{uv} = 18.5$, a flux limit of $1.35 \times 10^{-16}\,\mathrm{erg\,s^{-1}\,cm^{-2}\,\AA^{-1}}$. The second flux limit is that of the subsequent radio follow-up survey. We find this can

be well approximated by a central $0.20 \deg^2$ region with a 4σ sensitivity of $170\,\mu$Jy and an outer $0.75 \deg^2$ region with a sensitivity of $340\,\mu$Jy. The subsequent spectroscopic analysis of the UV-selected sample introduces further biases, as firstly only objects detected in the UV have any Hα (or redshift) information, and secondly only objects in our sample which lie at $z_{spec} \leq 0.4$, the redshift at which Hα is shifted out of our spectroscopic window, have information on this diagnostic line.

To study these selection criteria, we predict the expected number count distribution of our sample over the FOCA survey area as a function of apparent UV magnitude (m_{uv}) and redshift (i.e. $n(m_{uv}, z)dm_{uv}dz$) as

$$n(m_{uv}, z)dm_{uv}dz = \frac{\omega}{4\pi}\frac{dV}{dz}\phi(m_{uv}, z)p(m_{uv})dm_{uv}dz \qquad (4)$$

where $\phi(m_{uv}, z)$ is derived from the local (dust-uncorrected) UV luminosity function $\phi(M_{uv})$ (see Treyer et al. 1998, S2000), $p(m_{uv})$ is the spectroscopic completeness as given in S2000 and ω is the survey area in steradians.

For every galaxy in each (m_{uv}, z) bin, a variable and moderate dust extinction at $2000\,\text{Å}$ (A_{2000}) is then simulated, brightening the UV magnitudes by a random amount of $A_{2000} = 0 - 1\,$mag. To simulate the observational uncertainties, we apply a random "error" to each galaxy measurement based on the observational errors discussed in Section 2. To convert these dust-corrected UV magnitudes to an expected $1.4\,$GHz luminosity we use the ratio of the star-forming relations derived in Section 3.1. As a sanity check, we also compare this conversion value with the ratio of the characteristic luminosities (L_*) for the UV and $1.4\,$GHz LFs of star-forming galaxies, taken from S2000 and Mobasher et al. (1999) respectively, and find agreement to within a factor of two.

By studying the relation between the *dust-uncorrected* L_{uv} and the $L_{1.4}$ (derived from the *corrected* L_{uv}) the simulation predicts the form of the relationship on the $L_{1.4} - L_{uv}$ luminosity plane (including the effects of the observational uncertainties) we might expect to see if our radio survey were deep enough to detect all the FOCA galaxies (Figure 1).

The simulation is then used to identify areas of the diagnostic plot in which we do not find galaxies due to the selection effects of the sample by excluding those objects that fall below the sensitivity of the radio survey. The prediction from this simulation is compared in Figure 1 with the actual observed data. Also shown are the "accessible" areas of the diagram for galaxies at different redshifts based on the formal flux limits of the two surveys. Clearly we cannot detect the majority of the intrinsically low luminosity objects in this study because of the flux limit of the radio survey, and, for a given UV luminosity, those radio galaxies

we do detect in our simulation lie along the bottom of the distribution of model galaxies (i.e. have brighter $1.4\,$GHz luminosities). We are thus biased against objects at low intrinsic radio power but which are bright enough to be detected in the UV (i.e. faint star-forming or post-starburst objects). This can also be seen by examining the limits by redshift, where the model galaxies lie offset from the line denoting the respective survey limits. Extending the radio survey to fainter flux limits will shift the vertical lines in Figure 1 to the left, allowing a greater fraction of the UV galaxies to be detected at given redshift.

There is also a larger scatter in the observed data, compared to the simulation, which assumes the $L_{uv} - L_{1.4}$ conversion to be perfectly linear. Scatter in the simulations can be generated by varying the adopted dust extinction on the UV luminosities over larger ranges. However, if we increase the range of A_{2000} in this way, we brighten the predicted radio luminosities and end up with an excess population c.f. the observations. For example, 14% of the UV galaxies are detected at $\geq 4\sigma$; with $A_{2000} = 0$ the predicted fraction of UV galaxies detected in the radio is $\sim 4\%$, for $A_{2000} = 0 - 1$ the fraction is $\sim 10\%$, for $A_{2000} = 0 - 2$ the fraction is $\sim 20\%$ and for $A_{2000} = 1 - 2$ the fraction is $\sim 45\%$. Therefore, to generate a large scatter by varying the dust extinction over larger ranges results in the detection of a larger fraction of our UV population at $1.4\,$GHz than is actually observed. We will return to this subject in Section 4.3.

In summary, the simulations in this section reflect the presence of a bias against low power radio sources with moderate dust extinction, which will not appear in our UV survey. However, our conclusion from Figure 1 is that this bias will not significantly affect our results as it does not exclude populations of objects with significantly different properties or luminosities to those that are detected.

3.3. Observational Results

With the above selection effects in mind, we now consider the UV/Hα/$1.4\,$GHz relations. The UV, Hα, and $1.4\,$GHz luminosities, uncorrected for dust extinction, are compared in Figure 2 for galaxies which have such available data. FOCA galaxies without a reliable radio detection are shown as upper limits in radio luminosity. Figure 2 demonstrates apparent correlations between different SF diagnostics over $3 - 4$ orders of magnitude, as predicted from Section 3.2.

We test the strength of these correlations using various statistical methods. We calculate the linear correlation coefficient (or "Pearson's r"), as well as the non-parametric Spearman rank-order correlation coefficient (see Table 3). In these tests between any two datasets, a

result of $+1$ indicates a perfect, positive correlation, -1 indicates a perfect negative correlation, and 0 indicates that the two sets of data are uncorrelated. In all cases the results are > 0.65, with most > 0.8, indicating a significant correlation between these SF diagnostics. Additionally, the $L_{H\alpha}$–$L_{1.4}$ relation appears to be better correlated than L_{uv}–$L_{1.4}$.

To fit the correlations, we perform a least squares fit weighted by the errors in both variables to be correlated. We list the resulting χ^2, probability of χ^2, and the fitted slopes and errors in Table 3. We note there is a large scatter about these best-fit lines (Figure 2) – with up to an order of magnitude difference between the SFRs derived from different diagnostics – and systematic offsets from the lines of constant SFH.

As expected if the 1.4 GHz fluxes reliably trace the SF free from dust extinction, galaxies are under-luminous in Hα and UV when compared to the 1.4 GHz luminosity. Also, there appears to be luminosity dependencies in Figure 2 (most pronounced in the UV/1.4 GHz plot) in the sense that the brighter radio sources are more under-luminous in UV, as shown by the slopes of the best-fit lines. This effect is not seen to such a large extent in the $L_{H\alpha}$–$L_{1.4}$ plot, though the effect may still be present to some degree. It is unclear whether this luminosity-dependent effect reflects a non-linearity in the relationship between radio flux and SF or a greater degree of extinction in more energetic systems. This is quantitatively similar to the situation found by Cram et al. (1998) for a larger, although less homogeneous, sample.

The effect of dust on the Hα and UV luminosities is a major source of uncertainty. In our previous work (S2000), in galaxies where both Hα and Hβ were detected, nebular emission lines were corrected using the Balmer decrement, and these Balmer-derived corrections then extended into the UV using a Calzetti et al. (2000) reddening law (see also Calzetti 1997). An average of these Balmer corrections was then used in galaxies where Hβ was not detected at an adequate S/N. After corrections based on the Balmer decrement have been applied (Figures 3a and 3b), the SFRs derived from the different diagnostics agree rather better. However, the Hα/UV luminosities are still generally under-luminous when compared to 1.4 GHz luminosities, and the systematic effects and scatter seen before dust correction remain (Table 3).

We investigate the significance of the scatter seen in these plots in two ways. Firstly, we compare the residuals of the 1.4 GHz luminosities from the weighted best-fit lines with the measurement errors in the radio luminosities. Whilst the residuals show a flat distribution over the range $0 - 1.5$ (in log luminosity), the distribution of the errors is markedly different, being strongly peaked in the range $0 - 0.4$ (again in log-luminosity units). A similar pattern is found for the dust-corrected Hα and UV measurements. Secondly, we note that the straight line fitting results (Table 3) generally give *poor* fits to the data for the $L_{1.4}$-L_{uv} relation

(denoted by the χ^2 values), even though the datasets are undoubtedly correlated. This implies that either the observational errors are underestimated (a scenario we do not believe to be true) or that the scatter is larger than would be expected for a tight linear correlation. While the size of this sample is small, making these kinds of tests difficult, we nonetheless conclude that the scatter we see in these plots cannot arise purely from observational errors in our data (see also section 3.2).

We conclude that although the SF diagnostics correlate over several orders of magnitude, there is a large (approximately an order of magnitude) and statistically significant scatter around these correlations which is not removed after simple dust corrections. This implies that our best-fit correlations are not consistent with calibrations based on constant SFHs, a tight, linear $L_{1.4}$–SFR relationship, *and* extinction corrections which are independent of galaxy luminosity.

4. Discussion

In this section, we will discuss the implications of the results of Section 3.3 and try to resolve the apparent discrepancies highlighted there. The major features of the dataset are the offsets (and non-linearities) when compared to our standard scenario, and the scatter that we see around the best-fit lines of the correlations.

4.1. The Contribution of Active Galactic Nuclei

We start with the hypothesis that the non-linearity observed in Figure 2 is due to the inclusion of active galaxies, or at least objects where SF is not the dominant emission mechanism at radio frequencies (for example AGN, where the radio emission may be dominated by a nuclear "monster"). To investigate this, we search for evidence of different populations in the spectra of the galaxies: those with detected *narrow-line* Hα emission (i.e. *known* to be star-forming) and those with weak or non-existent Hα emission. We exclude those galaxies observed with the WIYN, where the spectral wavelength coverage is insufficient to detect Hα. Of the remainder, only one galaxy has no detectable Hα emission (formally a fraction of 4%, compared with $\sim 30\%$ in the FOCA sample as a whole), and it lies away from the remainder of the galaxies (marked on Figure 2). We see evidence that the 1.4 GHz luminosity varies as a function of $(UV - B)_0$ colour (with higher luminosity systems being bluer), and note that the object with no Hα is the reddest object in our sample ($\simeq 6.5$ c.f. a median $(UV - B)_0 \simeq 0$ for this sample). This is consistent with the scenario that objects

with little or no Hα emission are weakly star-forming or early-type galaxies, possibly hosting AGNs, which are responsible for the observed UV and 1.4 GHz luminosities.

No evidence is found for other significant AGN contamination (e.g. broad emission lines or unusual emission line ratios) in those objects with Hα emission (see S2000 for a fuller discussion; see also Contini et al. in preparation). We conclude that whilst there are undoubtedly AGN and non star-forming galaxies present in our sample, we find no evidence that they are responsible for the scatter and non-linearities in the observed relations.

4.2. Non-linearities in the diagnostics plots

One of most interesting results from this study is the slopes of the best-fit relations, which are significantly different from those expected, assuming constant SF scenarios (i.e. a slope of one, see Section 3.2). One possibility is using the Calzetti et al. (2000) extinction result to apply optical extinction measures (the Balmer ratio) at UV wavelengths is not appropriate for our sample of galaxies, for example if complex dust geometries ensured a non-trivial relation between Hα and UV attenuations. Until some independent measure of the UV extinction is available – for example measures at other UV wavelengths in addition to 2000 Å – such a possibility must be deferred to a later analysis. There appear to be two other possible explanations for these observed non-linearities (as well as non-uniformities in the SFH which we discuss in the next section); the related effect of a luminosity-dependent dust correction, and a non-linearity in the $L_{1.4}$–SFR calibration. We discuss each in turn.

Our previous dust corrections take little account of any possible luminosity dependence, as only few galaxies posses Hα, Hβ and 1.4 GHz emission. Such luminosity effects could arise if intensely star-forming galaxies (i.e. those with larger 1.4 GHz luminosities), or the star-forming regions of these galaxies, posses dustier environments. Wang & Heckman (1996) investigated such effects in a local sample of galaxies, and demonstrated that the UV(2000 Å)/FIR ratio decreases with increasing FIR luminosity, implying that the dust opacity may increase in more strongly star-forming environments. If such effects were present in our sample, then dust corrections which accounted for this would have the effect of 'rotating' our best-fit lines in an anti-clockwise direction.

To investigate this in more detail, we follow Hopkins et al. (2001) and attempt to derive a relation between the intrinsic SFR in a galaxy and the extinction present. Ideally, this could be done by examining the Hα/Hβ trend with a SF diagnostic unaffected by dust, e.g. the 1.4 GHz luminosity. Unfortunately, the sample size of objects with radio, Hα and Hβ detections is currently so small that such a comparison is not conclusive.

Instead, to explore the consequence of a luminosity dependence, we appeal to the full sample of S2000 galaxies (whether or not they have a radio detection in the present survey) and correlate the Hα/Hβ ratio with both *uncorrected* and *Balmer-corrected* Hα luminosity. We see a clear trend in both cases, with intrinsically brighter Hα luminosity galaxies having a larger Hα/Hβ ratio, even before dust correction of the Hα. We demonstrate this relationship in Figure 4. It is important to realize that this relationship has a large scatter (partly due to the uncertainties in determining the Hα and Hβ fluxes – see S2000), and so such corrections should only be used in a statistical manner.

By fitting the corrected relationship (weighted by the errors in both the Balmer ratio and the Hα luminosity), we are able to construct an observed relationship between the intrinsic SFR in an object (as governed by the corrected Hα emission) and the Balmer decrement, which can then be used for a subsequent dust correction. This fitted relationship is

$$\frac{\text{H}\alpha}{\text{H}\beta} = 0.82 \times \log(SFR) + 4.24. \tag{5}$$

and has a correlation coefficient of 0.65. Hopkins et al. (2001) use this technique, but derive the SFRs independently from FIR observations. This approach is obviously to be preferred, as the FIR provides a measure of the intrinsic SFR independently from the Hα measure used above. They find Hα/Hβ = 0.80 × log(SFR) + 3.83, in remarkably good agreement with the above estimate despite differences in sample selection and the SF diagnostic used to determine the dust-corrected SFR. Therefore, for each object detected in our radio survey – i.e. with an independent measure of (presumed) dust-free SF at 1.4 GHz – we can correct the observed Hα and UV luminosities using equation (6) and a Calzetti et al. (2000) law to extend to UV wavelengths. Obviously, such an approach can only correct the general trend seen in our sample, and will not remove the galaxy to galaxy scatter.

The resulting correlations are shown in Figure 5. The slope of the best-fit line is now closer to unity (predicted in constant SF scenarios and with linear 1.4 GHz to SFR conversions), though the UV/1.4 GHz relation is still slightly too shallow. Adopting the Hopkins et al. (2001) correction gives an almost identical result. Larger and deeper samples are clearly needed with a more comprehensive wavelength coverage, but this first analysis suggests that empirical, luminosity-dependent extinction corrections can go some way to explaining the slopes of our best-fit relations.

The second explanation considers the validity of the calibration of the 1.4 GHz luminosities and the conversion into a SFR. This calibration is based on the observed conversion values of the non-thermal radio luminosity to the supernova rate of our own galaxy. If, in small (or low-SFR) galaxies, cosmic ray electrons were able to escape more easily than in

larger systems, or at least have a different escape fraction compared to our galaxy, one may underestimate the radio-derived SFR in low luminosity systems, and possibly overestimate in high-luminosity systems (see for example Chi & Wolfendale 1990; Condon et al. 1991). Such an effect could generate a similar 'luminosity-dependent' effect to that observed. A full analysis of this complex issue must await a more complete dataset.

4.3.   The physical origin of the scatter

The second major feature in our data is the statistically significant scatter around the best-fit lines. As we saw in Section 3.2, generating this scatter via an increased range of dust extinctions in our sample raises difficulties in reconciling the radio-detected fraction of UV galaxies with those expected in simulations (assuming a Calzetti et al. (2000) law). We investigate this effect in several ways by examining the variation of the Hα/UV ratio as a function of 1.4 GHz luminosity (Figure 6). This diagnostic diagram is the least sensitive to dust, affected only by *differential extinction* between Hα and the UV (assuming the radio data are dust free). Also included on Figure 6 is the position of each galaxy, using different extinction corrections, based on the Balmer decrement, the luminosity-dependent corrections and the range of corrections corresponding to visual extinctions of $A_V = 0.5, 1.0, 1.5$ & 2.0. Again, we adopt the Calzetti et al. (2000) law to extend the extinction corrections into the UV.

Figure 6 implies that, for a constant SFR, it is unlikely that dust or IMF variations (i.e. varying the upper mass cut-off) are sufficient to explain the scatter. Even considering the full range of dust corrections, some galaxies have Hα/UV ratios that cannot be reproduced. We conclude that while a significant fraction of the scatter in this diagram is due to different levels of dust extinction among the galaxies, these dust corrections cannot (in their present form) explain the entire dataset. Other more complex dust geometries, for example that of Charlot & Fall (2000) which models the time-varying attenuation of Hα line emission and UV continuum, will again be deferred to a later paper.

In S2000, a comparison of Hα and UV luminosities for the entire FOCA sample revealed discrepancies that were difficult to reconcile within the framework of simple dust corrections. Therefore, S2000 considered the possibility that a fraction of the FOCA galaxies were undergoing bursts of short-term, intensive SF, which were able to explain the observed dataset to a certain degree. Such scenarios naturally generate a scatter on the Hα/UV/1.4 GHz planes due to differing dependencies on the timescale of SF of these different diagnostics (see Section 3.1). For example, UV continuum radiation is present after the completion of a starburst for a longer duration than nebular or radio emission. By applying this hypothesis

to the current dataset, we attempt to explain the likely cause of the observed trends in Figure 2 and 3. Whilst this dataset is too small for a thorough quantitative analysis, we can nevertheless test the reliability of such approach. Therefore, we relax the assumption of a constant SFH and consider a temporally varying SFH for our field galaxies. This is done by superimposing exponential starbursts of varying strength and duration onto underlying exponential SFHs, as a function of time, thereby simulating a 'star-bursting + evolved population' galaxy, from which we can use PEGASE-II to estimate the evolution of the Hα, UV, and 1.4 GHz luminosities over time (see Section 3.1).

The effect of varying the burst parameters is demonstrated in Figure 6 by assuming different bursts corresponding to over reasonable ranges (5–35% and 10–110 Myr duration). The bursts occur at a galactic age of 6 Gyr. For illustrative purposes, each artificial galaxy has a mass of 10^{10} M$_\odot$, of course in reality this is unlikely to be true, but we must await near-IR data to explore this further. It is clear that all of the scatter could be explained in terms of a temporally varying SFHs using bursts of different parameters, though with this small sample size it is not possible to constrain the burst parameters in any meaningful manner.

5. Conclusions

We have presented the first results from a decimetric radio survey of nearby galaxies, with the ultimate goal of comparing SF diagnostics for a homogeneous sample of star-forming galaxies. We find broad correlations over several orders of magnitude between the different SF diagnostics but with a large galaxy-to-galaxy scatter and offsets/non-linearities from relations predicted using simple dust extinction and SF scenarios. By dividing our sample into two (those with and without *detected* Hα emission), we tentatively conclude that the scatter and offsets that we see are not due to a significant non-starforming population of galaxies.

We find evidence for luminosity-dependent effects in our dataset, and show that luminosity dependent dust corrections or a mis-calibration of the 1.4 GHz-SFR calibration, or a combination of both, can go some way to resolving this effect. We also demonstrate that, over realistic ranges, differential extinction between galaxies cannot be solely responsible for the scatter in our relations; indeed our dataset argues against significant extinction in our sample. We conclude the discrepancies between different SF diagnostics can only be partly explained by simple models of dust extinction in galaxies. These models cannot by themselves explain all the observed differences, introducing the need for temporally varying SFHs and/or more complex models of extinction, to explain the entire dataset.

REFERENCES

Baugh, C. M., Cole, S., Frenk, C. S., & Lacey, C. G. 1998, ApJ, 498, 504

Bell, E. F. & Kennicutt, R. C. 2001, ApJ, 548, 681

Blain, A. W., Smail, I., Ivison, R. J., & Kneib, J. 1999, MNRAS, 302, 632

Calzetti, D. 1997, in The Ultraviolet Universe at Low and High Redshift: Probing the Progress of Galaxy Evolution, 403

Calzetti, D., Armus, L., Bohlin, R. C., Kinney, A. L., Koornneef, J., & Storchi-Bergmann, T. 2000, ApJ, 533, 682

Charlot, S. & Fall, S. M. 2000, ApJ, 539, 718

Charlot, S. & Longhetti, M. 2001, in press, MNRAS, astroph/0101097

Chi, X. & Wolfendale, A. W. 1990, MNRAS, 245, 101

Cole, S., Lacey, C. G., Baugh, C. M., & Frenk, C. S. 2000, MNRAS, 319, 168

Condon, J. J. 1992, ARA&A, 30, 575

Condon, J. J., Anderson, M. L., & Helou, G. 1991, ApJ, 376, 95

Condon, J. J. & Yin, Q. F. 1990, ApJ, 357, 97

Cowie, L. L., Songaila, A., & Barger, A. J. 1999, AJ, 118, 603

Cram, L., Hopkins, A., Mobasher, B., & Rowan-Robinson, M. 1998, ApJ, 507, 155

Eisenhauer, F. 2001, in "Starbursts: Near and Far", ed. L.J. Tacconi and D. Lutz, astroph/0101321

Fioc, M. & Rocca-Volmerange, B. 1999, in astro-ph, astro–ph/9912179

Gallego, J., Zamorano, J., Aragon-Salamanca, A., & Rego, M. 1995, ApJ, 455, L1

Gilmore, G. 2001, in "Starbursts: Near and Far", ed. L.J. Tacconi and D. Lutz, astroph/0102189

Glazebrook, K., Blake, C., Economou, F., Lilly, S., & Colless, M. 1999, MNRAS, 306, 843

Haarsma, D. B., Partridge, R. B., Windhorst, R. A., & Richards, E. A. 2000, ApJ, 544, 641

Hopkins, A. M., Connolly, A. J., Haarsma, D. B., & Cram, L. E. 2001, in press, AJ, astroph/0103253

Kennicutt, R. C. 1998, ARA&A, 36, 189

Lilly, S. J., Le Fevre, O., Hammer, F., & Crampton, D. 1996, ApJ, 460, L1

Madau, P., Ferguson, H. C., Dickinson, M. E., Giavalisco, M., Steidel, C. C., & Fruchter, A. 1996, MNRAS, 283, 1388

Milliard, B., Donas, J., Laget, M., Armand, C., & Vuillemin, A. 1992, A&A, 257, 24

Mobasher, B., Cram, L., Georgakakis, A., & Hopkins, A. 1999, MNRAS, 308, 45

Moorwood, A. F. M., van der Werf, P. P., Cuby, J. G., & Oliva, E. 2000, A&A, 362, 9

Pei, Y. C., Fall, S. M., & Hauser, M. G. 1999, ApJ, 522, 604

Rowan-Robinson, M., et al. 1997, MNRAS, 289, 490

Salpeter, E. E. 1955, ApJ, 121, 161

Scalo, J. 1998, in ASP Conf. Ser. 142: The Stellar Initial Mass Function, ed. G. Gilmore & D.Howell (San Francisco: ASP), 201

Somerville, R. S., Primack, J. R., & Faber, S. M. 2001, MNRAS, 320, 504

Steidel, C. C., Adelberger, K. L., Giavalisco, M., Dickinson, M., & Pettini, M. 1999, ApJ, 519, 1

Sullivan, M., Treyer, M. A., Ellis, R. S., Bridges, T. J., Milliard, B., & Donas, J. . 2000, MNRAS, 312, 442

Tresse, L. & Maddox, S. J. 1998, ApJ, 495, 691

Treyer, M. A., Ellis, R. S., Milliard, B., Donas, J., & Bridges, T. J. 1998, MNRAS, 300, 303

Wang, B. & Heckman, T. M. 1996, ApJ, 457, 645

This preprint was prepared with the AAS LaTeX macros v5.0.

Table 1.   The details of the different samples in our combined survey.

Sample	Total (vsad)	Total (imfit)	Total (pixel-sum)	Total	Total (with Hα)[2]	Total (with fluxed Hα)[3]
Largest sample	26	25	3	**54**	30	(21)
(minus > 1 POSS counterparts)	23	21	3	**47**	27	(19)
(minus Coma galaxies)[1]	22	18	3	**43**	25	(17)

[1]Corresponding to the default sample used in the analysis

[2]Excludes WIYN galaxies with insufficient spectral coverage to detect Hα

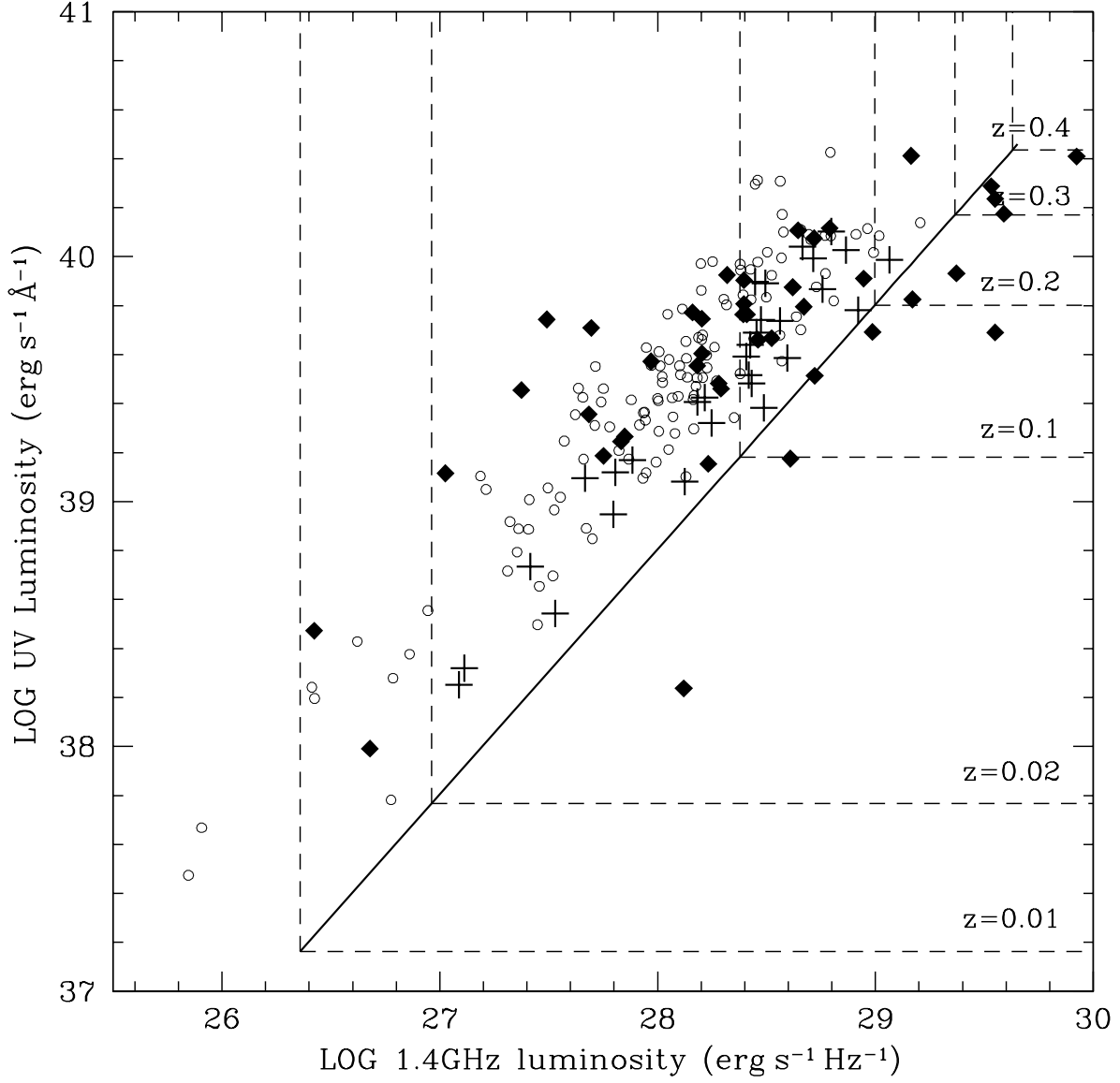[3]WHT observed galaxies with adequate flux calibration

Fig. 1.— An investigation of the limitations of a joint radio and UV survey of star forming galaxies. Circles illustrate the likely distribution of a UV-selected sample according to source count and redshift data obtained for the $m_{UV} < 18.5$ FOCA sample, a hypothetical $L_{1.4} - L_{uv}$ correlation, observational errors and a randomly distributed extinction (see text for details). Crosses show those UV sources that would be detected to the flux limit of the present VLA survey. The dashed lines indicate the formal regions (above and to the right), in which a galaxy at a particular redshift can be found based on the UV and radio survey limits. Overplotted (solid diamonds) is the actual observational data.
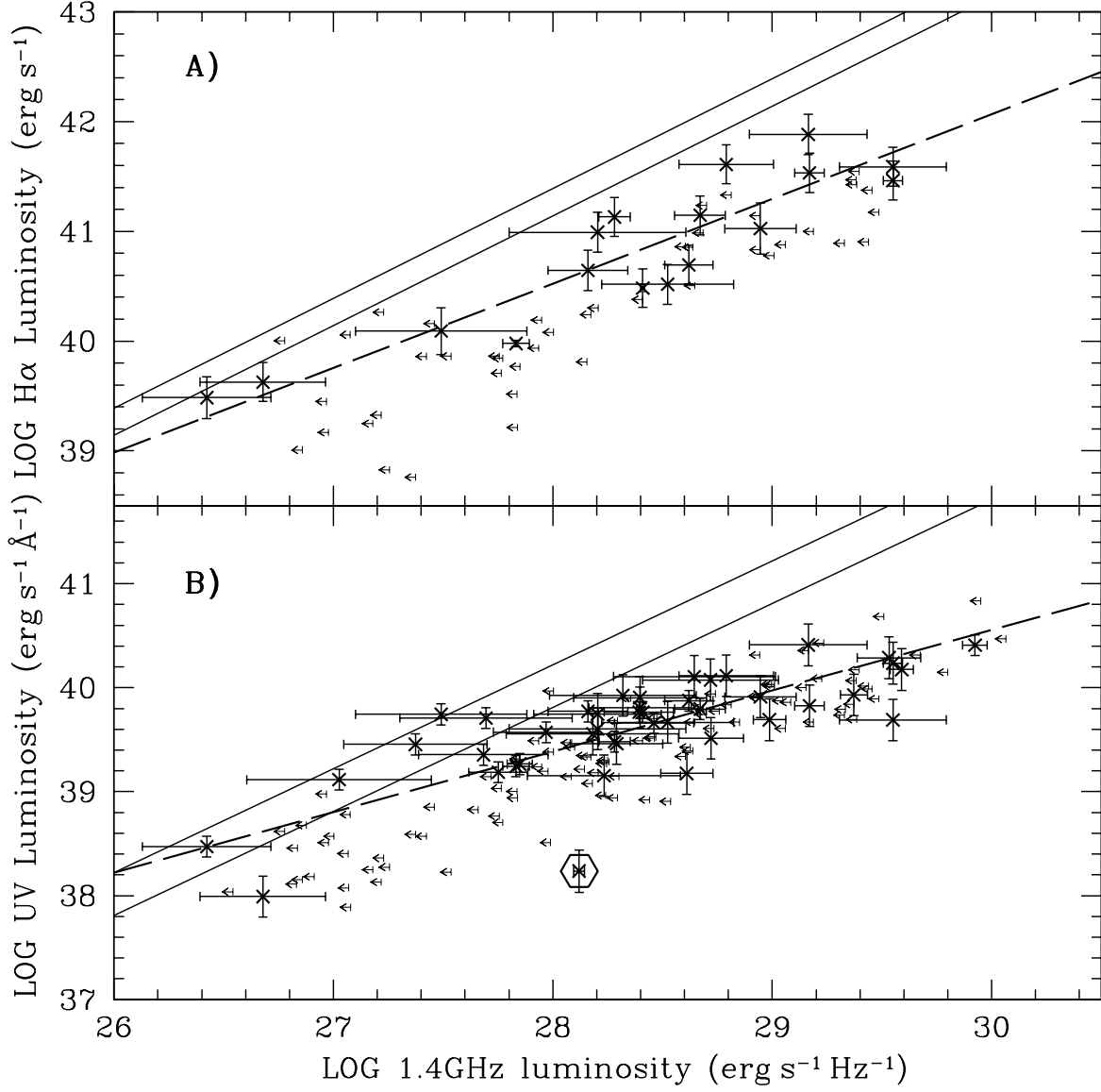
Fig. 2.— The correlations between the different SF tracers. **A)** The correlation between radio and Hα luminosities, **B)** between radio and UV luminosities. In both cases, the two solid lines denote equality of SFRs for $Z = 0.02$ and $\tau = 100$ Myr (UPPER LINE) and $Z = 0.004$, $tau = 10$ Myr (LOWER LINE), indicating the range of uncertainties in the luminosity-SFR conversion. Values are taken from Table 2. Both **A** and **B** show observed values which have not been corrected for dust extinction. In both diagrams, the long-dashed lines show the least-squares best-fit to the galaxies. The boxed galaxy in **B** indicates an extremely red object compared to the other galaxies in the sample.
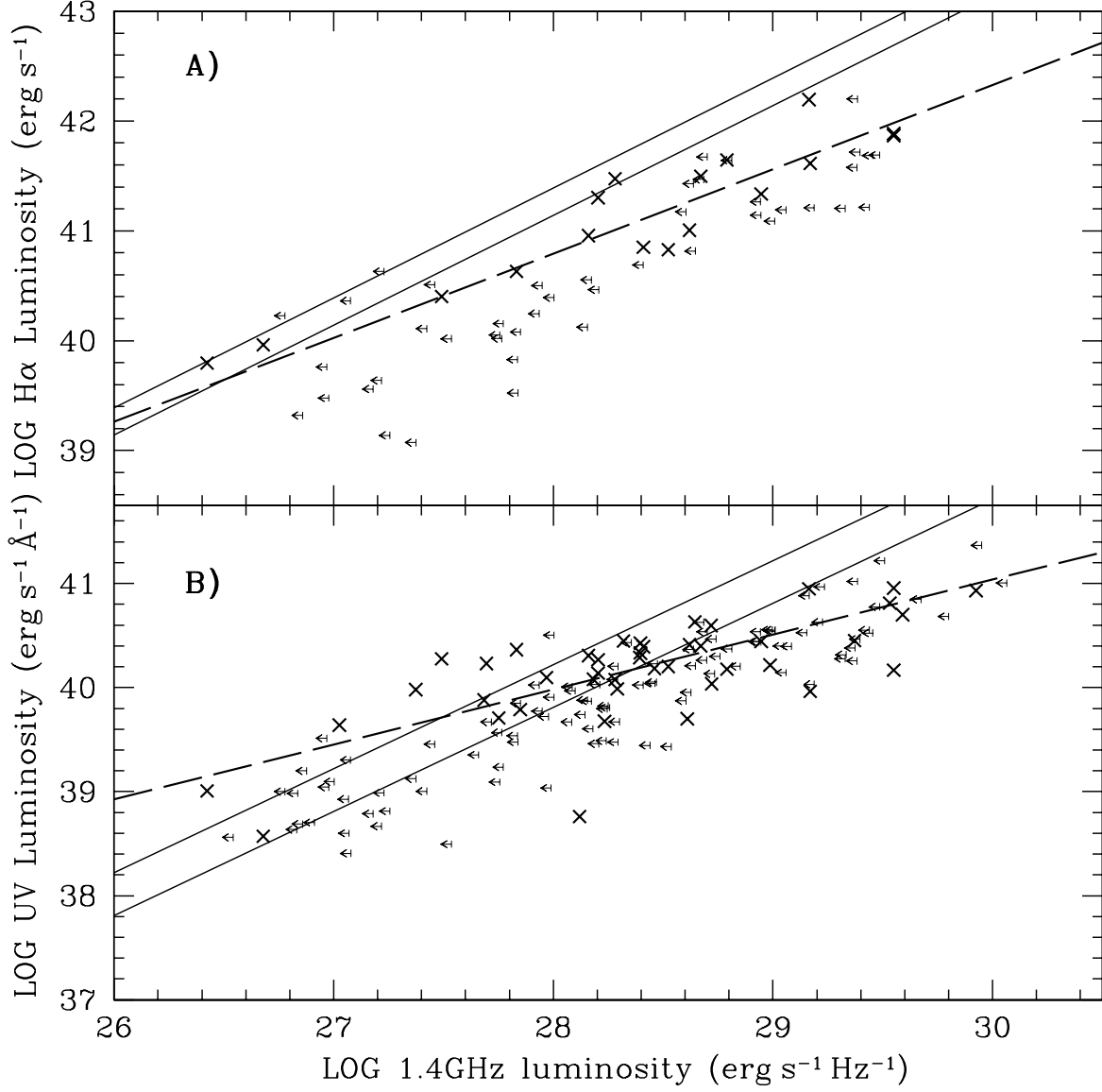
Fig. 3.— As Fig. 2, but with the Hα and UV luminosities corrected for dust as in S2000 (based on the Balmer decrement), and with error bars removed for clarity.
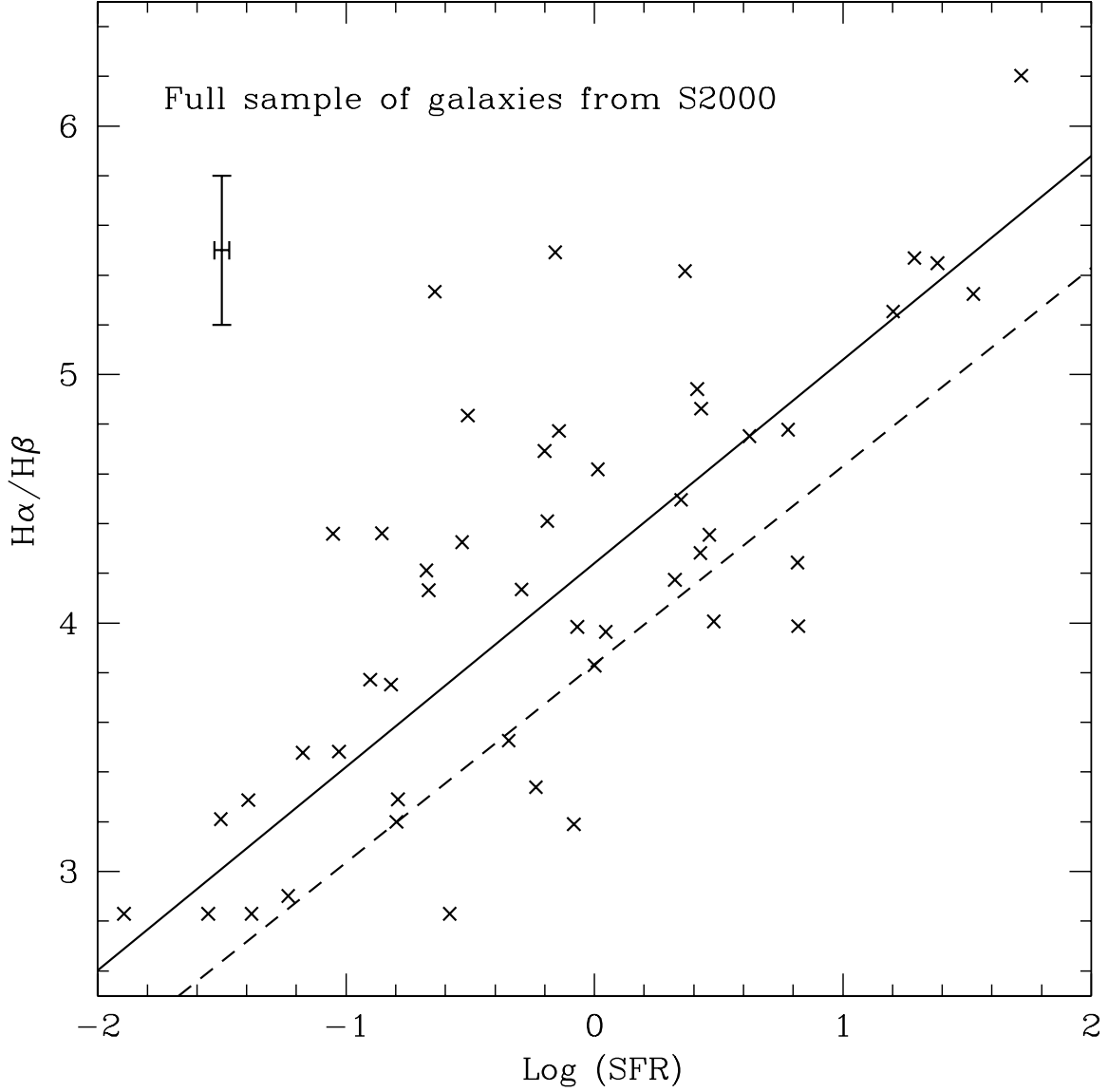
Fig. 4.— The ratio of Hα to Hβ as a function of SFR derived from dust corrected Hα luminosities. The points are from the full spectroscopic sample of S2000, regardless of whether they have a radio detection in this present survey. The solid line indicates the weighted least-squares best fit to the dataset; the dashed line shows the relationship derived by Hopkins et al. (2001) for an independent sample of galaxies. The error-bar in the top left corner demonstrates the median errors in the two parameters correlated.
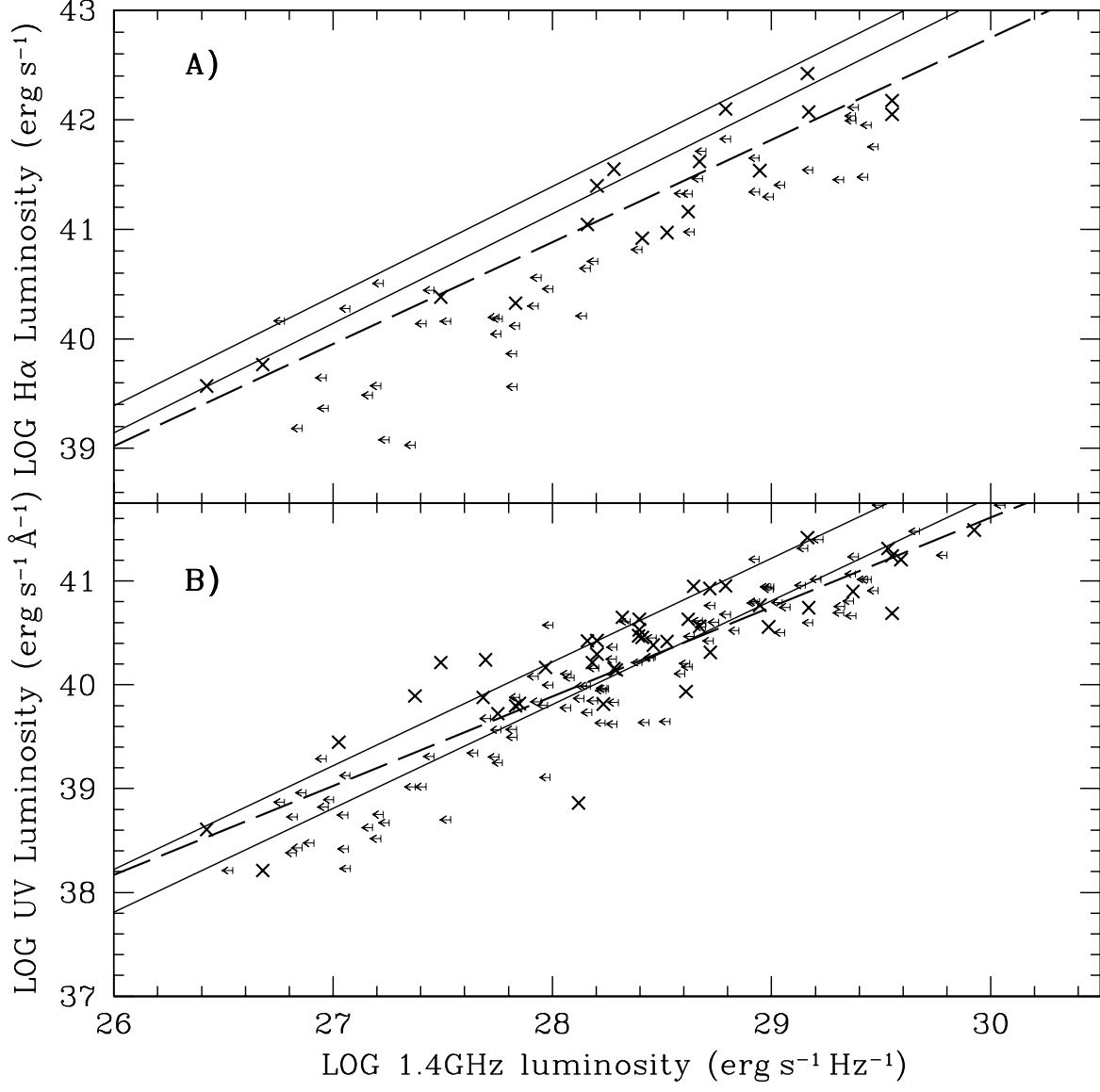
Fig. 5.— As Fig. 2, but with the Hα and UV luminosities corrected according to a luminosity dependent extinction prescription, again with error bars removed for clarity.
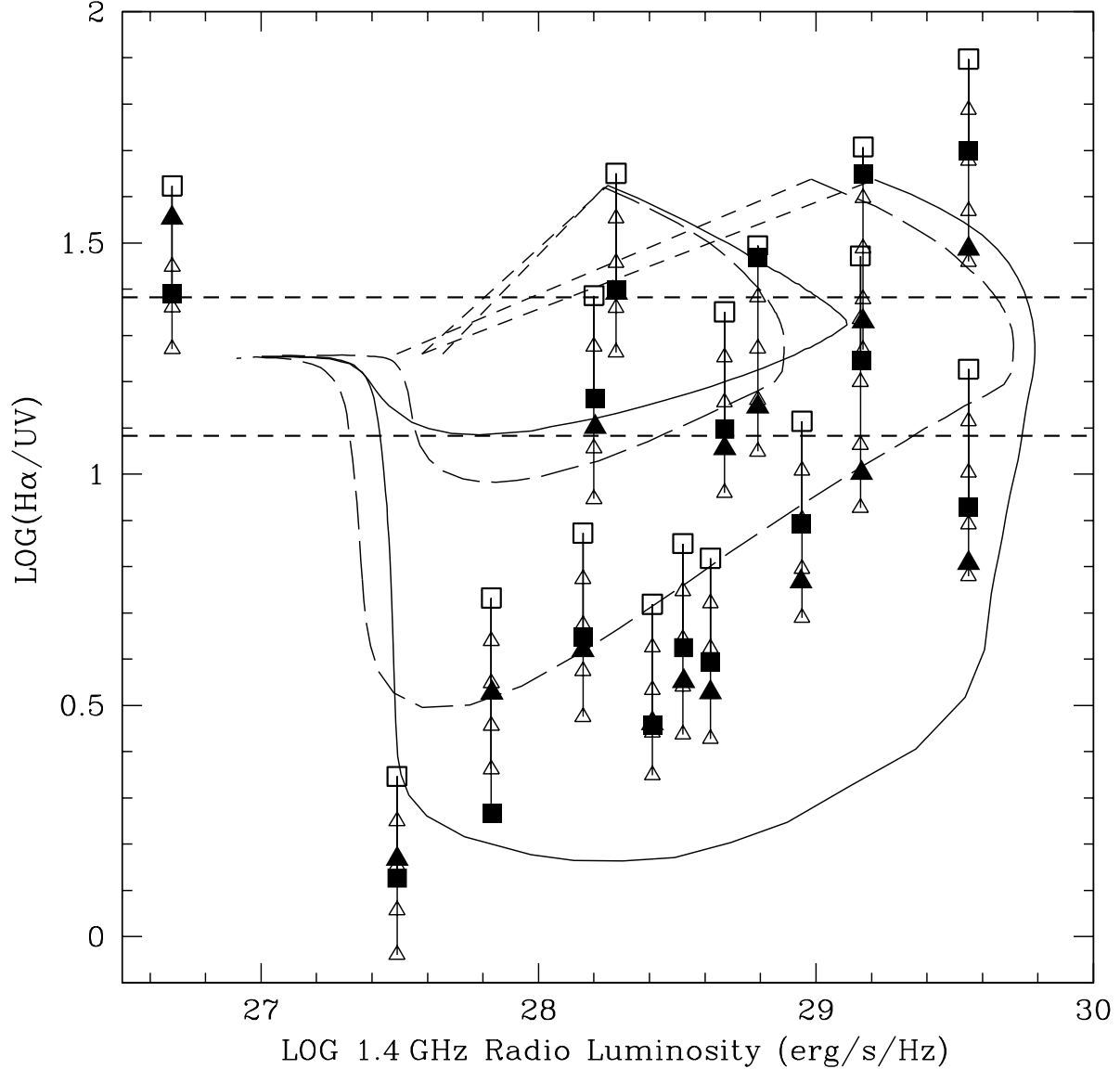
Fig. 6.— The variation in the Hα/UV ratio with 1.4 GHz luminosity for our sample galaxies. OPEN SQUARES: galaxies with no extinction corrections applied, FILLED SQUARES: Extinction corrections from S2000, FILLED TRIANGLES: Corrections based on a luminosity-dependent prescription, OPEN TRIANGLES: Extinctions with $A_V = 0.5, 1.0, 1.5$ & 2.0. The horizontal dashed lines show the range of values obtained by varying the IMF upper mass cutoffs from $125 \, \mathrm{M}_\odot$ (top) to $50 \, \mathrm{M}_\odot$ (bottom). We also show predictions based on bursts of SF superimposed on exponential SFHs. Here, the solid lines represent bursts of duration $110 \, \mathrm{Myr}$ (small loop) and $10 \, \mathrm{Myr}$ (large loop), mass 20% in both cases. The long dashed lines represent bursts of mass 5% (small loop) and 35% (large loop), duration $30 \, \mathrm{Myr}$ in both cases. The short dashed lines are areas at the start of the burst where galaxies would spend an extremely small amount of time, they then move clockwise around the loops over time.

Table 2.   Factors derived to convert diagnostic luminosities into SFRs for various luminosities and timescales, in the sense $\mathrm{SFR}(\mathrm{M}_\odot\,\mathrm{yr}^{-1})$=Luminosity/conversion factor.

| Z | $H\alpha$ | UV $(\mathrm{erg\,s^{-1}\,\AA^{-1}})$ | | | $1.4\,\mathrm{GHz}$ $(\mathrm{erg\,s^{-1}})$ | |
	$(\mathrm{erg\,s^{-1}})$	$10\,\mathrm{Myr}$	$100\,\mathrm{Myr}$	$1000\,\mathrm{Myr}$	$10\,\mathrm{Myr}$	$100\,\mathrm{Myr}$
0.0004	$2.02\mathrm{e}^{41}$	$3.24\mathrm{e}^{39}$	$5.87\mathrm{e}^{39}$	$7.68\mathrm{e}^{39}$	$2.03\mathrm{e}^{27}$	$8.84\mathrm{e}^{27}$
0.004	$1.67\mathrm{e}^{41}$	$3.39\mathrm{e}^{39}$	$5.84\mathrm{e}^{39}$	$7.24\mathrm{e}^{39}$	$2.06\mathrm{e}^{27}$	$1.08\mathrm{e}^{28}$
0.02[1]	**$1.22\mathrm{e}^{41}$**	**$3.75\mathrm{e}^{39}$**	**$5.76\mathrm{e}^{39}$**	**$6.56\mathrm{e}^{39}$**	**$2.39\mathrm{e}^{27}$**	**$8.85\mathrm{e}^{27}$**
0.05	$0.87\mathrm{e}^{41}$	$3.86\mathrm{e}^{39}$	$5.49\mathrm{e}^{39}$	$5.95\mathrm{e}^{39}$	$3.28\mathrm{e}^{27}$	$8.78\mathrm{e}^{27}$

[1]Corresponding to solar metallicity and the default conversion factors used in the analysis

Table 3.   The Diagnostic Correlations

Relation	Dust Correction	Number of Sources	Correlation Coeff.[1]	Spearman Coeff.[1]	χ^2	χ^2 Probability[2]	Slope
$H\alpha$-radio	None	17	0.908	0.873	38.9	0.0007	0.73 ± 0.07
UV-radio	None	43	0.752	0.745	101.4	< 0.0001	0.58 ± 0.05
$H\alpha$-radio	Balmer decrement	17	0.927	0.900	20.5	0.155	0.77 ± 0.06
UV-radio	Balmer decrement	43	0.711	0.634	136.2	< 0.0001	0.53 ± 0.05
$H\alpha$-radio	Lum-dependent	17	0.936	0.884	33.4	0.0024	0.93 ± 0.07
UV-radio	Lum-dependent	43	0.865	0.877	84.1	< 0.0001	0.85 ± 0.05

[1]Where 1 equals a perfect positive correlation, 0 indicates no correlation

[2]Where smaller values indicate poorer fits